

The Influence of Electrolyte Volume on Calendaric Aging of Lithium-Ion Batteries

Sebastian Klick,* Gereon Stahl,* and Dirk Uwe Sauer

Lithium-ion cells with graphite anodes and nickel–manganese–cobalt oxide (NMC622) cathodes are filled with three different amounts of electrolyte. During formation, incremental capacity analysis indicates small differences in the formation processes between cells with insufficient electrolytes to fill all pores and those with an electrolyte volume above the total pore volume of the cell. Complimentary analysis of the gases developed during formation shows that the composition of these cells differs from the cells with a sufficient electrolyte. The aging of cells under high temperature (60 °C) and high constant voltage of 4.2 V is studied. During aging, cells with higher amounts of electrolyte degrade substantially slower. Based on data available from electrical tests, a theory explaining the volume-dependent rise of resistance and capacity decay is proposed.

1. Introduction

Optimized electrolytes enable cells with increased lifetimes and performance. However, optimizing electrolyte formulations is often a rather slow process as many different aspects and the complex interplay between reaction products formed at anode and cathode, respectively, need to be considered. Furthermore, the volume of electrolyte has an impact on the specific price of lithium-ion cells as it adds costs without contributing to the storable energy of the cell.

Thus, optimization of the electrolyte is subject to current research.^[1] We propose a new approach to accelerate the testing

of new electrolytes and investigate the question of whether a lower electrolyte volume in cells can help in lowering the costs. Additionally, cells differing only with respect to the electrolyte volume enable differentiating electrolyte-related aging processes from other causes of degradation.

Assuming that electrolyte degradation is influenced by the concentration of solvable products of side reactions on anode and cathode, respectively, a reduction of the electrolyte volume would accelerate the degradation of the cell. The initial degradation reactions are limited by the surfaces of anode and cathode, respectively. The solvable products of these reactions can diffuse through the electrolyte potentially causing


further reactions.^[2–4] Thus, the concentration of degradation products would rise faster in cells with lower amounts of electrolyte. Therefore, degradation in these cells should be accelerated unless the reaction is a rare zeroth order reaction.^[5] If aging is not accelerated, cells with lower electrolyte volumes could be used to reduce costs and increase energy density.

Furthermore, other effects related to electrolytes with insufficient stability on either anode or cathode could also be accelerated: lower electrolyte volume reduces the electrolyte reservoir, thus accelerating dry-out due to electrolyte consumption.^[6] Dry-out could increase the path length for ions migrating from one electrode to the other, leading to similar effects as the geometric overhang observed in lithium-ion cells.^[7] The overhang is an area that slowly participates in the electrochemical processes in the cell due to its large distance from the active area.^[7] Thus, the overhang is slowly charged or discharged over the course of calendaric aging as the lithium distribution within the anode homogenizes. Furthermore, it is known that the electrolyte concentration changes over time.^[8] If this change results from reactions that are limited by the available active surface, it will also be accelerated, as cells with lower electrolyte volume contain less conductive salt and less solvent in absolute terms. An increase in salt concentration (due to solvent degradation) lowers the diffusivity and changes the conductivity of the electrolyte, while a decrease would increase diffusivity.^[9] The conductivity peaks at salt concentrations of about 1 molL^{−1} and decreases for lower and higher concentrations.^[10] In a comprehensive study, Landesfeind and Gasteiger^[11] investigated the effect of various temperatures and concentrations on the conductivity, transference number, diffusivity, and thermodynamic factors of exemplary electrolytes. Their results show that in commonly used electrolytes, conductivity does not change substantially between

S. Klick, G. Stahl, D. U. Sauer
ISEA RWTH Aachen
Campus-Boulevard 89, 52074 Aachen, Germany
E-mail: Sebastian.Klick@isea.rwth-aachen.de;
Gereon.Stahl@isea.rwth-aachen.de

D. U. Sauer
Helmholtz Institute Muenster (HIMS)
IEK-12
Forschungszentrum Juelich
Campus-Boulevard 89, 52074 Aachen, Germany

S. Klick, G. Stahl, D. U. Sauer
Jülich Aachen Research Alliance, JARA-Energy
Templergraben 55, Aachen 52065, Germany

 The ORCID identification number(s) for the author(s) of this article can be found under <https://doi.org/10.1002/ente.202300566>.

© 2023 The Authors. Energy Technology published by Wiley-VCH GmbH. This is an open access article under the terms of the Creative Commons Attribution License, which permits use, distribution and reproduction in any medium, provided the original work is properly cited.

DOI: 10.1002/ente.202300566

0.5 and 1.5 molL⁻¹ LiPF₆.^[11] Below and above these concentrations, conductivity is more sensitive to the concentration.

Electrolyte degradation reactions have been studied from different perspectives. Some publications mainly concentrate on reactions contributing to the formation of the solid-electrolyte-interphase (SEI),^[12] while others focus on electrolyte oxidation reactions^[13–15] or redox shuttles contributing to self-discharge.^[16,17]

During the formation process, the initial SEI is formed by the reduction of electrolyte components.^[18] An ideal SEI would passivate the anode and thus prevent any further electrolyte reduction on the anode interface.^[18] However, in real-life cells, the SEI continues to grow.^[18–20] Furthermore, delithiation of nickel–manganese–cobalt oxide (NMC) cathodes can destabilize the layered structure, contributing to electrolyte oxidation.^[15] Different reaction pathways have been proposed in recent publications showcasing the complex nature of chemical reactions within lithium-ion cells.^[13–15] Among the hypothesized products of these oxidation processes are water^[14] and HF.^[13] Water can further react with dissociation products of the often-used salt LiPF₆ to form HF.^[21] HF can be part of different degrading reactions in lithium-ion cells, such as attacking SEI components, e.g., lithium carbonate, or dissolving transition metals from the cathode, which in turn can react with SEI components.^[2–4,22]

As we aim to analyze the effects of different electrolyte volumes on the degradation of the battery cell, we will not look into various chemical reaction pathways in detail but focus on electrical data from the batteries. Other scholars also investigated variations of electrolyte volumes in lithium-ion cells: an often-used metric when comparing various electrolyte volumes is the filling or volume factor f of a cell.^[23,24] It is calculated by dividing the electrolyte volume $V_{\text{Electrolyte}}$ by the total pore volume V_{Pores} of the cell (see Equation (1)).

$$f_{\text{filling}} = \frac{V_{\text{Electrolyte}}}{V_{\text{Pores}}} \quad (1)$$

An et al.^[23] investigated cyclic aging of pouch cells (70 mAh, NMC532|Graphite) using different filling factors between 1.3 and 3.5. They concluded the optimal filling factor for these cells is 1.9. Cells below this filling factor showed faster degradation, whereas an increased filling factor did not improve cell performance. Günter et al.^[24] investigated different amounts of electrolyte under cyclic aging using NMC111|Graphite pouch cells. Using filling factors between 0.6 and 1.8, they found an optimal filling factor around 1.4. Their data show a faster degradation for cells with electrolyte volumes below this filling factor. The high-frequency resistance increases below a filling factor of 1.4. Interestingly, the capacity decreases for cells with a filling factor higher than 1.4. Günter et al.^[24] attribute this to excess VC and its decomposition reaction consuming lithium, which is then no longer available for reversible (de-)intercalation.

In this article, we investigate calendaric aging of lithium-ion cells with different amounts of electrolyte without any additives. We investigate whether electrolyte degradation and its effects on cell performance (e.g., dry out of active areas) can indeed be accelerated by reducing the amount of electrolyte in the cell. We aim to identify the influence of lower electrolyte volumes

on calendaric aging of lithium-ion batteries at 60 °C and a constant voltage of 4.2 V.

2. Results and Discussion

The results from the measurements of three different groups of cells are presented in this section. Cells of three groups (V21, V28, V35) only differ in the amount of electrolyte as described above.

2.1. Formation

The formation process is analyzed using incremental capacity analysis (ICA) of the formation charge cycle and EIS after formation. The measurements of the gas composition complement these results.

2.2. Insights from Electrical Data

The electrical data of the formation cycle are analyzed by calculating the incremental capacity of the initial charging process. The ICA was chosen over the differential voltage analysis (DVA) for the formation cycle because the measured capacity includes both SEI-forming and intercalation processes which hinder a proper comparison of DVA curves as the capacity is commonly used as the x -axis. ICA is usually analyzed with respect to the voltage which additionally facilitates the identification of potentials of certain reactions. The dQ/dV -plot in **Figure 1a** shows that differences between the groups V35 and V28 do not significantly exceed the variations between different cells within the same group. This indicates similar electrochemical processes and similar kinetics. However, cells of group V21 exhibited an additional peak in the high-voltage domain at roughly 3.9 V. This indicates an additional or different formation process, which could lead to a different SEI.

Data gathered by electrochemical impedance spectroscopy displayed in **Figure 1c** show that the charge transfer resistance is significantly higher for cells in group V21. This supports the hypothesis that different formation reactions occurred in cells of group V21.

The capacity as measured during the C/20-capacity check after formation is similar for all cells in groups V35 and V28. The third group (V21) has a slightly lower capacity. The distribution of the capacities measured as part of the RPT can be seen in **Figure 1**.

2.3. Gas Analysis

The results from gas analysis also demonstrate a deviation between V21 and the other two groups. For analysis, the total amount of carbon-containing gas species in the gas sample was calculated to normalize the respective concentration values. The results are shown in **Figure 1b**. The share of ethylene which is a marker for EC reduction is higher for cells in groups V35 and V28, whereas the share of alkanes and carbon monoxide is higher for group V21. This indicates that there are indeed different formation reactions as suggested by the electrical data.

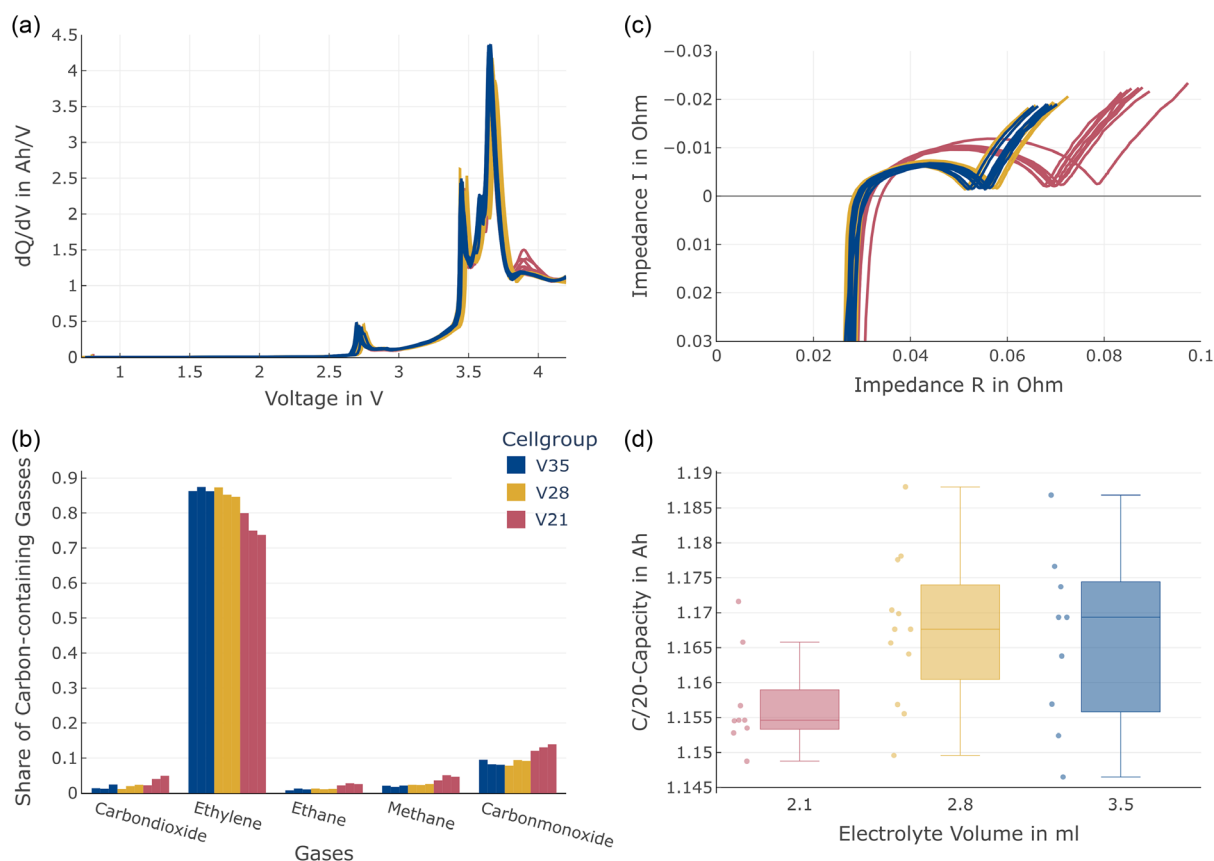


Figure 1. a) ICA curves of the formation cycle, b) gases evolved during formation normalized to the total carbon-containing gas species, c) EIS spectra after the initial RPT after formation, and d) the initial C/20 discharge capacity after formation.

2.4. Calendaric Aging

During calendaric aging, cell capacity fades. The observed decrease in capacity for the three cell groups will be discussed in the following section, followed by DVA, to investigate the contributions of loss of active material and loss of cyclable lithium, respectively. Finally, EIS will give further insights into the aging mechanism.

2.5. Capacity Decay

The initial capacity of the cells showed only minor deviations in an order of 30 mAh (see Figure 1). However, the capacity loss strongly depends on the electrolyte volume. Figure 3 depicts the absolute capacity loss during the two periods of aging comparing both the C/20 and C/2 capacities, respectively. The C/20 capacities are also displayed in Figure 2, showing a clear dependency between the capacity decay and the initial electrolyte volume.

The boxplots in Figure 3 show that for cells with 2.1 mL electrolyte the median lost capacity amounts to roughly 375 mAh during the first period and 367 mAh in the second period for C/2. Thus, the aging rate does not increase substantially. The C/20 capacity shows a different picture: in this case, the median of the lost capacity is 300 mAh during the first period

and increases to 353 mAh in the second period. These differences could be related to an increased initial inhomogeneity for the cells of group V21, as their filling factor is below one. Thus, the electrolyte volume is not sufficient to wet all pores. Under higher current (C/2), parts that are not well-wetted in the initial cell are not used to their full extent. Thus, the increasing capacity fade is omitted at higher currents due to areas with an increased ionic resistance (e.g., due to thin electrolyte films) which are not used with higher currents, but influence the available capacity when cycling at C/20.

In V28, no such difference occurs. Capacity loss is roughly the same for C/20 (182 and 179 mAh, respectively) and slightly increases for C/2 (222 and 206 mAh, respectively). No acceleration of aging is observed. In the case of V35, the lost capacity during the first period is higher and slows down in the second period. One possible explanation could be the geometric overhang that becomes fully charged during the first aging period. Thus, the capacity that can be used for regular cycling is lost during this initial period.^[7] For the other two groups, the overhang effect could mask an increase in irreversible capacity decay during the second period of aging. During the initial period, some of the capacity is lost to the overhang. Thus, the irreversible capacity loss is lower than measured. In the second period, the aging accelerates due to dry-out.

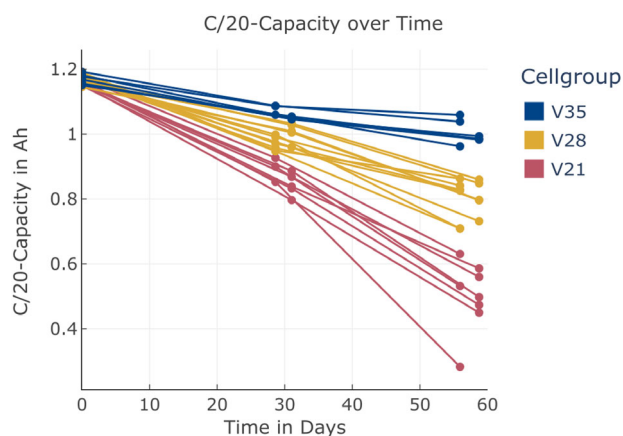


Figure 2. Capacities over time for each cell. The colors mark the initial electrolyte volume filled into the cell.

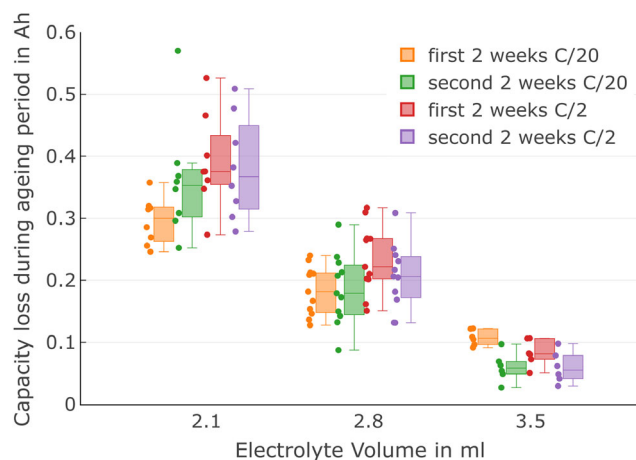


Figure 3. Capacity loss during the high-temperature-high-potential ageing periods for the three cell groups and the two C-rates tested in the RPT. Capacity loss increases with decreasing electrolyte volume.

Over 4 weeks of high-temperature-high-voltage storage, the cells in group V21 exhibited a capacity decay of about 60% to 85%, whereas the cells in group V28 lost “only” about 30% to 50% of their initial capacity. The third group with the highest electrolyte volume performed best with a loss of about 10%. It has to be noted that capacity decay includes both capacity loss due to increased impedances as well as those related to the loss of cyclable lithium and available active material. However, the contribution of increased impedances at low current rates of C/20 should be negligible.

2.6. Differential Voltage Analysis

DVA can be used to trace different degradation mechanisms.^[25] In this case, a low-current qOCV (C/20 based on nominal Capacity of 1 Ah) in both charge and discharge direction is performed to be able to compare the differences between these two processes.

Figure 4 shows the DVAs after formation and the two phases of high-temperature-high-potential aging. During the initial qOCV, the curves are well aligned with only small differences between the three groups of cells. Notably, in the case of group V21, one can see some slow relaxation behavior affecting the discharge process at high states of charge. These slow processes could indicate a more relevant role of slow diffusion processes, e.g., solid-state

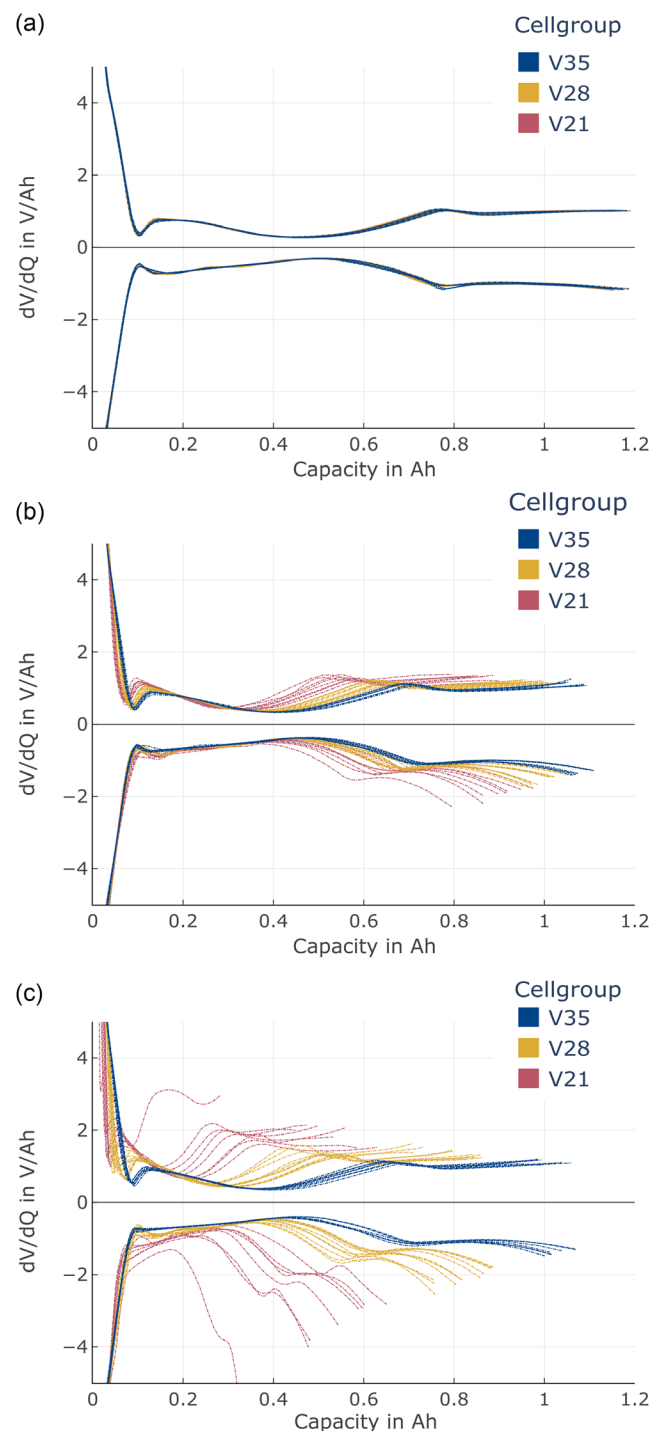


Figure 4. DVA curves of charge and discharge after a) formation, b) 2 weeks, and c) 4 weeks of high-temperature-high-voltage aging.

diffusion in these cells. The peaks in the DVA curve that can be attributed to phase changes within the graphite anode are all in good alignment. This means at low C-rates, the available anode capacity is very similar for all cells. From the negligible differences between the graphs on the dV/dQ axis, we conclude that the available cathode capacity is also similar in all fresh cells.

Over the course of aging, the peak marking of the transition from LiC_{12} to LiC_6 ^[25] shifts to lower capacities indicating loss of available active anode material. Furthermore, the differential voltage at high SOC increases. This part of the DVA curve represents changes at the cathode. An increase means that higher states of lithiation are reached faster. Therefore, we assume this to be an indicator of the loss of available active cathode material. Both aging modes are most pronounced for the cells in group V21. Furthermore, the slow diffusion process at high SOC during discharge already observable at the initial measurement in group V21 becomes more relevant for all cells. This effect is more pronounced in cells with lower electrolyte volume.

Interestingly, the Coulombic efficiency during the qOCV cycle grows over aging, as displayed in **Figure 5**. This effect is more prominent for cells of group V21. In aged cells, it approaches values substantially larger than 1. One possible cause of this effect could be the higher internal resistance of these cells, and slower relaxation kinetics leads to a higher SOC at the end of the initial discharge prior to the qOCV cycle. While this SOC offset is one explanation, another one could be found in the overhang areas of the cells, as they are calendarically aged at 100% SOC. The geometric overhang is a part of the cell connected by rather long ionic diffusion paths.^[7] Dry-out or the formation of gas bubbles might also create areas within the cell that are only connected over a long diffusion path with the active areas, thus creating additional aging-induced “overhang”. The two mechanisms will affect the DVA curves in different ways: while an offset of SOC will not affect the distance between the graphite features on the capacity axis, the overhang-effect should charge the active area of the cell, especially at SOC lower than the storage SOC, thus reducing the distance of the graphite features. The latter could also be attributed to aging phenomena (loss of active anode material). Thus, we can separate these effects by comparing the distance of said features during charging and discharging. Aging-induced changes

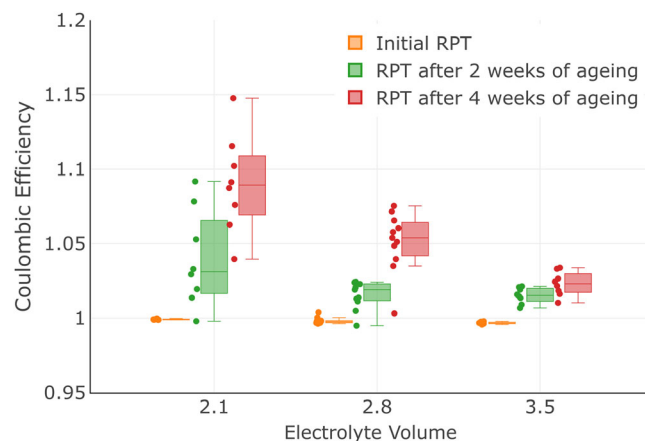


Figure 5. Coulombic efficiencies of the three groups of cells during the qOCV cycle of the RPT.

should be the same for both cases, whereas overhang-induced currents increase the distance during discharging and decrease the distance during charging. Unfortunately, the low-SOC-graphite features are not clearly visible in cells for group V21 after 4 weeks, hence, the analysis can only be performed for cells of the other two groups. Indeed the difference in the peak distance between charge and discharge increases from roughly 23% during the initial RPT to about 10% after 4 weeks of high-temperature–high-voltage aging in the case of cells of group V28 with a difference of about 5% after 2 weeks of aging (see **Figure 6**). This indicates a growing section of the cell which is only electrochemically active with rather slow time constants.

To facilitate the comparison of DVA curves of cells at very different states of health, the differential voltage was normalized to the measured capacity. In this representation, a change of cell balancing (e.g., due to loss of active material on one electrode, or loss of lithium) will cause an obvious shift of the features of the curve. However, in the case of the cells investigated here, we find that the DVA curves normalized to measured capacity behave strikingly similar (see **Figure 6**). The peak shifts discussed above can also be identified and are marked with the red arrows in **Figure 6**. As the balancing of the cell does not change substantially, we conclude that the cell mainly ages due to symmetric loss of available active materials on both anode and cathode. We would like to emphasize that loss of available active material could mean that it is not well-connected anymore (e.g., due to dry-out). The uniformity of the respective contributions of active material loss on anode and cathode, as well as loss of cyclable lithium suggests that dry-out is the dominant factor for aging in this case. If parts of the cell are not ionically connected anymore, e.g., due to a dried separator, both anode and cathode would lose roughly the same capacity. This would also explain the growing overhang, indicated by the growing distance of the $\text{LiC}_6/\text{LiC}_{12}$ transition peak between charge and discharge. It would also explain the observed increase in Coulombic efficiency to values substantially higher than one for cells with lower electrolyte volumes.

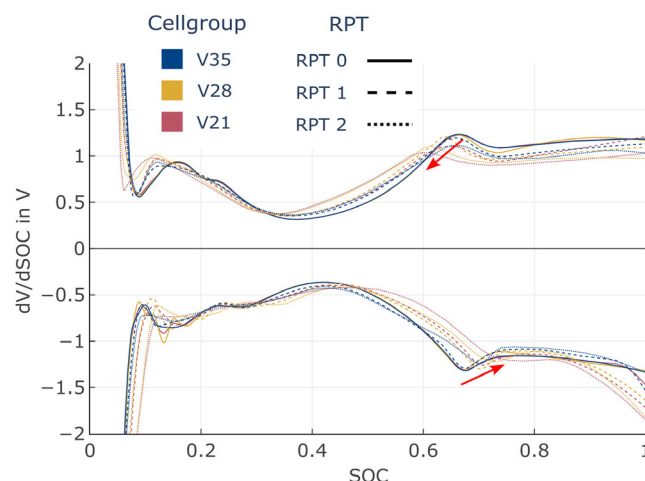


Figure 6. Selected DVA curves of one cell of each group over the RPTs. Medium-performing cells of groups V21 and V28 are displayed for comparison as these groups show substantial cell-to-cell deviation. Charge curves are in the positive and quadrant discharge in the negative one.

Dry-out of the cell thus seems to be an issue for cells with lower electrolyte amounts (V28, V21) with group V35 exhibiting only very minor capacity decay. Previously, we already discussed the differences in lost capacities over the aging period. Assuming dry-out as the main effect, we would suspect an increase in capacity decay once any surplus electrolyte is consumed. We assume that this increase in capacity decay rate is masked by lithium migration into the overhang during the initial aging period as discussed above.

2.7. Impedance Spectroscopy

EIS is used to measure frequency-dependent processes in lithium-ion cells. The impedance spectra are divided into four ranges during the analysis:^[26–28] inductance, serial resistance, the surface resistance, and diffusion processes. The different ranges are distinguished by the frequencies. In the high-frequency range, the serial resistance and inductance are measured. In the medium frequency range, surface resistances, charge transfer resistance, and/or SEI resistance dominate. Diffusion processes become visible in the lower frequency range. The focus of this article is on serial resistance and surface resistance. The point of intersection with the x-axis is referred to as the serial resistance. The serial resistance includes information about the ohmic resistance of the electrolyte and other contributions to the overall impedance. The surface impedance of the electrodes is identified by the size and shape of these semicircles in the impedance spectra in the middle-frequency range. A larger diameter indicates a higher charge transfer resistance, which can limit the cell's performance. This is related to processes such as electrode/electrolyte interfacial reactions, charge transfer kinetics, or surface passivation.^[26–28]

After the initial cycling, differences between group V21 and the other two groups (V28, V35) are immediately apparent in the impedance spectra, as shown in Figure 1. The impedance spectra of group V21 are shifted to the right on the x-axis compared to the other cells. An increased value on the x-axis in this context means an increased serial resistance. Even more apparent is that the semicircle for group V21 is broader. There are two possible explanations. First, the impedance depends on the active surface.^[10,29,30] It follows that after formation, areas of the electrode are already dry and thus electrochemically inactive. Second, the impedance depends on the chemical composition of the SEI.^[31–33] From the second approach, it follows that a chemically different SEI is created during the formation. The results from the gas analysis and the ICA of the formation data confirm that different chemical processes occur during formation. From the impedance data, it can be confirmed that reducing the amount of electrolyte from 2.8 to 3.5 mL has no effect on the electrochemical condition of the cells. After aging, the difference between the three groups becomes more apparent, as shown in Figure 7. The impedance correlates with the aging of the battery. It can be observed that the impedance of cells of V21 increases the most and at the same time the spread of the impedance is the greatest. The serial resistance and the charge transfer resistance increase. Cells that have a high internal resistance also have a high charge transfer resistance. This is especially evident in the V21 group. In contrast to the results from Figure 1,

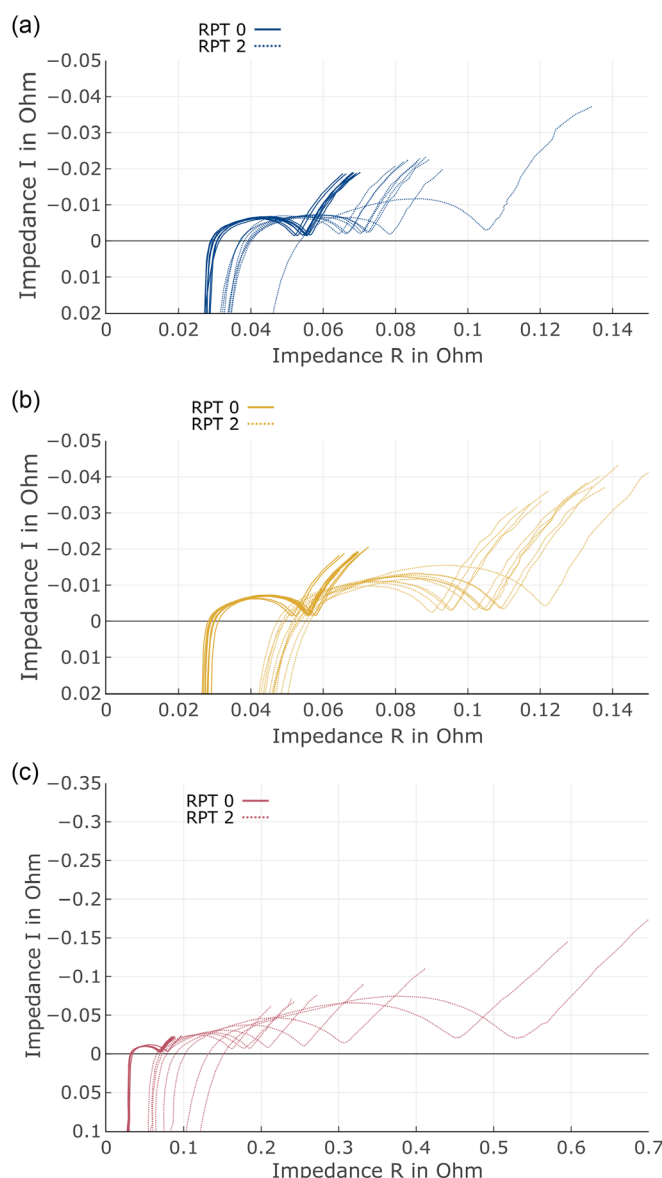


Figure 7. Comparison of impedance spectra after RPT 0 and RPT 2. a) V35, b) V28, and c) V21. The scale of the axis is different in each diagram to allow a meaningful comparison of the effects within each group.

significant differences after aging can be observed for cells of V28 and V35.

2.8. Linking of Impedance Rise and Capacity Fade

Assuming dry-out as the main factor for increased impedance and capacity decay, the two factors should be linked. Dry-out reduces the cross-section of ion-conducting paths through the pores of separators and electrodes. Additionally, the active surface area decreases due to dry-out. Particles that are not ionically connected anymore cannot contribute to the capacity of the cell. As mentioned above, changes in the salt concentrations could also affect the impedance of cells due to decreased ionic

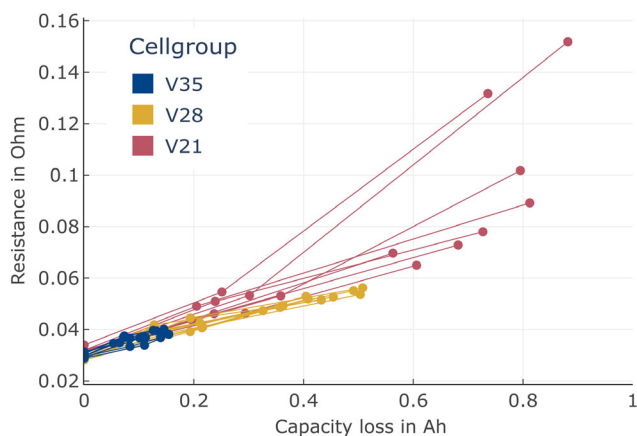


Figure 8. Resistance value of zero-crossing in the Nyquist diagrams of EIS measurements over capacity loss for the investigated cells.

conductivity and diffusivity of the electrolyte.^[11] Based on our measurements, we cannot rule out any such contribution. However, changes in salt concentration cannot explain the observed symmetric loss of active material on anode and cathode.

Using the zero-crossing in the Nyquist chart as a resistance value and the capacity values of the qOCV of the RPTs as a reference capacity, we can visualize the relationship between capacity loss and resistance increase (**Figure 8**). Cells of groups V28 and V35 follow a rather similar linear trajectory with similar gradients. Cells of group V21 show a slightly higher gradient indicating slightly different aging behavior. This difference could be related to the detected differences in SEI formation for this group of cells.

3. Conclusion

Electrolyte degradation and its influence on overall capacity decay and resistance rise are important but understudied issues. By investigating cells with the same chemistry but different electrolyte volumes, we explored the question of whether lower electrolyte amounts do accelerate aging.

The initial assumption that reducing the amount of electrolyte can accelerate aging has been validated for high-temperature-high-potential conditions. Both often-used aging metrics, capacity, and impedance degrade considerably faster in cells with reduced electrolyte volumes. By comparing results from DVA, capacity analysis, and impedance spectroscopy, we conclude that dry-out is the main driver of aging for all three groups of cells.

Our findings open up new opportunities for future research: the stability of a given electrolyte could possibly be analyzed using reduced electrolyte volumes to accelerate consequences of electrolyte instability such as dry-out. Additionally, using cells with different amounts of electrolyte can help to differentiate between aging processes that are mainly due to failure of active material (e.g., loss of electrical connection) and those that are part of the complex network of aging processes that are affected by the electrolyte. However, it is unlikely that one can simply extrapolate from cells with low amounts of electrolyte to those with larger volumes in any case. Günter et al.^[24] found that too much

vinylene carbonate (VC) can lead to loss of lithium during formation reducing the available capacity of the cell. Thus, one has to think carefully about the role of the respective additives to find out whether a comparison based on the absolute amount of additives or their concentrations is more helpful.

Another option arising from our research is the adaptation of the electrolyte volume to the use case of the battery as a way forward to widen the applications for lithium-ion batteries. For example, adding additional electrolytes for cells used in high-temperature conditions at high states of charge might alleviate some of the lifetime constraints at these conditions. Further research, using higher filling factors and different aging conditions, could shed some light on the dependency between aging conditions and optimal electrolyte volume.

4. Experimental Section

To compare cells with different electrolyte volumes, dry cells (1 Ah NMC622/Graphite, purchased from LiFun Technologies) were filled with different amounts of electrolyte (EC/EMC 5:7). Prior to filling, the cells were cut open and dried under dynamic vacuum at 80 °C.

To analyze the required drying time, one cell was cut open and placed in the drying oven, and weighed after 1, 2, and 5 days. While the cell was ≈0.01 g lighter after one day the weight of the cell did not change between day one and day five. Hence, it is assumed that the cell is sufficiently dry after one day under a dynamic vacuum at 80 °C. This time was then used to dry the cells for this study.

$$V_{\text{Pores, total}} = \sum_i V_i \cdot \Phi_i \quad (2)$$

The pore volume of the cells was calculated based on the porosity and volume of the cell components as provided by the manufacturer using Equation (2) with i = anode, cathode, separator, and V as the respective coating volume, and Φ as the respective porosity given by the manufacturer. It amounts to 2.26–2.37 mL. The manufacturer recommends 3.5 mL of electrolyte per cell. This corresponds to a filling factor of about 1.5, which is slightly higher than the optimal value identified by Günter et al.^[24] but substantially lower than the optimal value found by An et al.^[23] After drying, cells are filled with different amounts of electrolyte (3.5, 2.8, and 2.1 mL) corresponding to filling factors of 1.5, 1.2, and 0.9, respectively. We will refer to the three groups of cells by V35 (3.5 mL), V28 (2.8 mL), and V21 (2.1 mL), respectively. V21 has insufficient electrolytes to fill all pores of the cells. Filling and sealing of the cells were done in a nitrogen-filled glovebox with tightly controlled water content (below 0.3 ppm). The cells were not exposed to ambient air between drying and sealing.

The filled cells were kept at 1.5 V for at least 12 h to allow the electrolyte to properly wet the pores of the cells. For the formation cycle, the cells were clamped between two steel plates fixed with four M3 screws, tightened with a torque of 0.5 Nm at 80 °C. The formation cycle consists of a rest period of 8 h at open circuit conditions, followed by a constant current charge up to 4.2 V, and a subsequent constant current discharge to 3.9 V with an 8 h rest period afterward. The cells were degassed after formation and gas samples were taken and analyzed for three cells of each group. A gas sample is extracted from the gasbag of the cell using a gas-tight syringe. 50 µL of gas is then injected into a GC–MS-detector (Perkin Elmer Clarus 690 GC). This approach does not allow the quantification of the absolute gas amount, but the concentrations of different gas species can be compared.

After formation, the cells undergo a reference performance test (RPT) procedure consisting of an initial discharge, followed by a C/20 qOCV charge and discharge, a C/2-capacity measurement, and pulse tests at 50% SOC as measured by the C/2-capacity measurement. C-rates are calculated based on the cells' nominal capacity (1 Ah). Following this,

initial RPT cells are cycled for eight cycles with a current rate of C/5 to check Coulombic efficiency after formation. Subsequently, the cells are stored at a constant voltage of 4.2 V in an oven at 60 °C. The voltage was kept constant using a Hameg HM8143 power supply. The RPT is repeated after 2 weeks of storage under these conditions. Additional tests including electrochemical impedance spectroscopy (EIS; Zahner Zennium XC) and self-discharge measurements complement the insights from the RPT. We have measured the impedance spectroscopy potentiostatically with an amplitude of 5 mV in the frequency range from 1 MHz to 10 mHz. Cells spend \approx 2 weeks at room temperature before another 2 weeks of high-temperature–high-voltage hold was applied. It is assumed that the aging during the tests at room temperature is negligible compared to the degradation during the high-temperature–high-potential aging at 4.2 V and 60 °C.

Acknowledgements

The authors gratefully acknowledge the financial support by the Federal Ministry of Education and Research through the projects E-FlOa (BMBF03XP0349A), Meet-HiEnD III (BMBF03XP0258C), and BatgasMod (BMBF03XP0311B). The authors would like to thank Harsha Vardhan Sathyabalu for his support regarding the impedance spectroscopy measurements.

The range has been corrected on November 6, 2023, with addition of en dash after original online publication (Initially, the values did not have en dash for the range, so it read 2.262.37 mL).

Open Access funding enabled and organized by Projekt DEAL.

Conflict of Interest

The authors declare no conflict of interest.

Data Availability Statement

The data that support the findings of this study are available from the corresponding author upon reasonable request.

Keywords

calendaric aging, electrochemical impedance spectroscopy, electrolyte, electrolyte volume, lithium-ion cells

Received: May 26, 2023

Revised: August 2, 2023

Published online: October 30, 2023

- [1] X. Ma, J. E. Harlow, J. Li, L. Ma, D. S. Hall, S. Buteau, M. Genovese, M. Cormier, J. R. Dahn, *J. Electrochem. Soc.* **2019**, 166, A711.
- [2] N. V. Faenza, Z. W. Lebens-Higgins, P. Mukherjee, S. Sallis, N. Pereira, F. Badway, A. Halajko, G. Ceder, F. Cosandey, L. F. J. Piper, G. G. Amatucci, *Langmuir* **2017**, 33, 9333.
- [3] A. T. S. Freiberg, J. Sicklinger, S. Solchenbach, H. A. Gasteiger, *Electrochim. Acta* **2020**, 346, 136271.
- [4] X. Yang, J. Chen, Q. Zheng, W. Tu, L. Xing, Y. Liao, M. Xu, Q. Huang, G. Cao, W. Li, *J. Mater. Chem. A* **2018**, 6, 16149.
- [5] K. A. Connors, *Chemical Kinetics: The Study of Reaction Rates in Solution*, John Wiley & Sons, Hoboken, NJ **1990**.
- [6] R. Li, S. O'Kane, M. Marinescu, G. J. Offer, *J. Electrochem. Soc.* **2022**, 169, 060516.
- [7] M. Lewerenz, G. Fuchs, L. Becker, D. U. Sauer, *J. Energy Storage* **2018**, 18, 149.
- [8] M. K. G. Bauer, J. Harlow, T. Hynes, J. R. Dahn, *J. Electrochem. Soc.* **2023**, 170, 030543.
- [9] B. Ravikumar, M. Mynam, B. Rai, *J. Phys. Chem. C* **2018**, 122, 8173.
- [10] M. Ecker, T. K. D. Tran, P. Dechent, S. Käbitz, A. Warnecke, D. U. Sauer, *J. Electrochem. Soc.* **2015**, 162, A1836.
- [11] J. Landesfeind, H. A. Gasteiger, *J. Electrochem. Soc.* **2019**, 166, A3079.
- [12] S. K. Heiskanen, J. Kim, B. L. Lucht, *Joule* **2019**, 3, 2322.
- [13] Y. Zhang, Y. Katayama, R. Tatara, L. Giordano, Y. Yu, D. Fraggadakis, J. G. Sun, F. Maglia, R. Jung, M. Z. Bazant, Y. Shao-Horn, *Energy Environ. Sci.* **2020**, 13, 183.
- [14] R. Jung, M. Metzger, F. Maglia, C. Stinner, H. A. Gasteiger, *J. Electrochem. Soc.* **2017**, 164, A1361.
- [15] B. L. D. Rinkel, D. S. Hall, I. Temprano, C. P. Grey, *J. Am. Chem. Soc.* **2020**, 142, 15058.
- [16] S. E. Sloop, J. B. Kerr, K. Kinoshita, *J. Power Sources* **2003**, 119–121, 330.
- [17] T. Boulanger, A. Eldesoky, S. Buechele, T. Taskovic, S. Azam, C. Aiken, E. Logan, M. Metzger, *J. Electrochem. Soc.* **2022**, 169, 040518.
- [18] K. Xu, *Chem. Rev.* **2014**, 114, 11503.
- [19] P. M. Attia, W. C. Chueh, S. J. Harris, *J. Electrochem. Soc.* **2020**, 167, 090535.
- [20] F. Single, A. Latz, B. Horstmann, *ChemSusChem* **2018**, 11, 1950.
- [21] M. Stich, M. Göttlinger, M. Kurniawan, U. Schmidt, A. Bund, *J. Phys. Chem. C* **2018**, 122, 8836.
- [22] J. S. Edge, S. O'Kane, R. Prosser, N. D. Kirkaldy, A. N. Patel, A. Hales, A. Ghosh, W. Ai, J. Chen, J. Yang, S. Li, M.-C. Pang, L. B. Diaz, A. Tomaszewska, M. W. Marzook, K. N. Radhakrishnan, H. Wang, Y. Patel, B. Wu, G. J. Offer, *Phys. Chem. Chem. Phys.* **2021**, 23, 8200.
- [23] S. J. An, J. Li, D. Mohanty, C. Daniel, B. J. Polzin, J. R. Croy, S. E. Trask, D. L. Wood, *J. Electrochem. Soc.* **2017**, 164, A1195.
- [24] F. J. Günter, C. Burgstaller, F. Konwitschny, G. Reinhart, *J. Electrochem. Soc.* **2019**, 166, A1709.
- [25] P. Keil, A. Jossen, *J. Electrochem. Soc.* **2017**, 164, A6066.
- [26] J. Illig, M. Ender, A. Weber, E. Ivers-Tiffée, *J. Power Sources* **2015**, 282, 335.
- [27] P. Shafei Sabet, G. Stahl, D. U. Sauer, *J. Power Sources* **2020**, 472, 228189.
- [28] J. Illig, M. Ender, T. Chrobak, J. P. Schmidt, D. Klotz, E. Ivers-Tiffée, *J. Electrochem. Soc.* **2012**, 159, A952.
- [29] J. Landesfeind, J. Hattendorff, A. Ehrl, W. A. Wall, H. A. Gasteiger, *J. Electrochem. Soc.* **2016**, 163, A1373.
- [30] J. Costard, J. Joos, A. Schmidt, E. Ivers-Tiffée, *Energy Technol.* **2021**, 9, 2000866.
- [31] J. C. Burns, N. N. Sinha, G. Jain, H. Ye, C. M. VanElzen, W. M. Lamanna, A. Xiao, E. Scott, J. Choi, J. R. Dahn, *J. Electrochem. Soc.* **2012**, 159, A1105.
- [32] J. C. Burns, R. Petibon, K. J. Nelson, N. N. Sinha, A. Kassam, B. M. Way, J. R. Dahn, *J. Electrochem. Soc.* **2013**, 160, A1668.
- [33] R. Petibon, C. P. Aiken, N. N. Sinha, J. C. Burns, H. Ye, C. M. VanElzen, G. Jain, S. Trussler, J. R. Dahn, *J. Electrochem. Soc.* **2012**, 160, A117.